Research Square

Preprints are preliminary reports that have not undergone peer review.
They should not be considered conclusive, used to inform clinical practice,
or referenced by the media as validated information.

Electroweak-Scale Majorana Neutrino Masses and Precision Phenomenology from Generalized Geometric Misalignment

Weifeng Wang

wang_w01@yahoo.com

Jinhua Academy of Zhejiang Chinese Medical University, Jinhua, China https://orcid.org/0009-0008-5406-5690

Research Article

Keywords: Neutrino physics, Beyond the Standard Model, Neutrino mass, Majorana neutrino, Generalized geometric misalignment, Precision phenomenology, Non-unitary mixing, Flavor mixing, CP violation, LSND, MiniBooNE, MicroBooNE, MEG II, ATLAS, DUNE, Hyper-K

Posted Date: April 13th, 2026

DOI: https://doi.org/10.21203/rs.3.rs-9261148/v2

License: This work is licensed under a Creative Commons Attribution 4.0 International License.
Read Full License

Additional Declarations: The authors declare no competing interests.

Electroweak-Scale Majorana Neutrino Masses and Precision Phenomenology from Generalized Geometric Misalignment

Weifeng Wang

Jinhua Academy of Zhejiang Chinese Medical University, Jinhua, China

Contact author: wangweifeng@zhezhonglab.ac.cn; wang_w01@yahoo.com

Abstract

In this study, we explore the phenomenological implications of the renormalizable geometric misalignment (RGM) framework, which we recently proposed to naturally generate Majorana neutrino masses at the electroweak scale. Built upon a small misalignment between the $SU(2)$ gauge representation space and the chiral fields, this purely geometric approach achieves the sub-eV degenerate masses without relying on high-scale energies or severe fine-tuning. To accommodate full flavor mixing and CP-violating phases, we generalize the original RGM model by promoting the real, diagonal misalignment matrix $\mathbf{\Theta}$ to a complex and off-diagonal form. Comparing the non-unitary predictions from this extended theory against the recent experimental data reveals that the precision constraints, specifically the 2025 MicroBooNE null result, the 2025 $\mu^+ \to e^+\gamma$ decay limit from MEG II and the 2024 ATLAS W-decay universality measurement, favor the highly suppressed natural regime ($|\mathbf{\Theta}| \sim 10^{-7}$) over the high-mixing scenario ($|\mathbf{\Theta}| \sim 10^{-1}$). We further analyze the one-loop radiative corrections to the induced non-unitarity parameter and confirm that it is radiatively stable, consistent with 't Hooft's naturalness criterion. Finally, we discuss the implications of the intermediate regime ($|\mathbf{\Theta}| \sim 10^{-3} - 10^{-2}$) wherein the geometry-induced non-unitary mixing effects can serve as practical targets for future precision tests.

1 Introduction

In a recent work, the author proposed a renormalizable geometric misalignment (RGM) mechanism that successfully generates degenerate Majorana masses for left-handed (LH) and right-handed (RH) neutrinos at the electroweak scale [1]. The framework does not rely on either high energy scales or new heavy particles to suppress the neutrino masses [2, 3, 4, 5]. Instead, it introduces a purely geometric misalignment between the $SU(2)$ gauge representation space and the chiral neutrino fields to achieve the sub-eV masses. As a significant extension, the present work generalizes the original real, diagonal misalignment matrix $\mathbf{\Theta}$ to a complex and off-diagonal matrix, such that the theory can accommodate flavor mixing as well as the CP-violating phases.

In contrast to the standard high-scale models [6, 7, 8] where fine-tuning is required for heavy suppression, the RGM framework renders the smallness of the misalignment parameter ($|\mathbf{\Theta}| \ll 1$) technically natural. Based on 't Hooft's criterion [9], a small physical parameter is theoretically justified if its vanishing limit enhances the symmetry of the system. In our approach, taking the limit $\mathbf{\Theta} \to 0$ leads to the complete alignment between the $SU(2)$ gauge representations and the chiral fields. This geometric alignment results in the massless neutrinos and thus restores the global lepton number conservation. In this paper, we will demonstrate that the induced non-unitary mixing is radiatively stable up to high energy scales due to this symmetry protection.

While the symmetry protection ensures the theory's stability, it is essential to physically test the viability of the model. Hence, we confront the present extended model with the latest 2024–2025 precision experimental data. Specifically, we utilize the 2025 MicroBooNE null result [10, 11], the 2025 $\mu^+ \to e^+\gamma$ decay limit from MEG II [12, 13] and the 2024 ATLAS lepton universality measurement [14] to discriminate the highly suppressed natural regime ($|\mathbf{\Theta}| \sim 10^{-7}$) from the high-mixing scenario ($|\mathbf{\Theta}| \sim 10^{-1}$). The natural regime seamlessly yields a 0.05 eV Majorana mass scale with electron-like Yukawa couplings ($Y \sim 10^{-6}$). However, its non-unitary effects turn out to be too small for direct observation. Thereby, we identify a flavor-dependent intermediate regime ($|\mathbf{\Theta}| \sim 10^{-3} - 10^{-2}$) that safely evades current precision bounds while retaining the diagonal non-unitary mixing large enough to be probed by next-generation facilities.

The remainder of this paper is organized as follows. Section 2 details the formalism of the generalized geometric misalignment and the mass generation mechanism. Section 3 explores the phenomenological implications of the geometry-induced non-unitary mixing and zero-distance flavor transitions, and confronts different misalignment regimes with the LSND and MiniBooNE anomalies [15, 16, 17, 18] and the latest MicroBooNE null result. Section 4 assesses the constraints imposed by precision physics, specifically lepton radiative decay and W-boson universality. A proof of radiative stability, derived from the one-loop renormalization group equation, is provided in section 5. Finally, section 6 dis-

cusses the implications of the intermediate regime for future long-baseline (LBL) experiments, namely the Deep Underground Neutrino Experiment (DUNE) [19, 20] and the Hyper-Kamiokande (Hyper-K) [21, 22, 23], followed by the concluding remarks in section 7.

2 Formalism of Generalized Non-Universal Misalignment

2.1 The Generalized Interaction Lagrangian

Following our preceding work on the RGM framework [1], we start with the renormalizable Yukawa interaction involving the flavor doublets ψ'^{d}, the Higgs doublet and the CP-conjugate singlets $(\nu'^{s})^{c}$ (rather than the standard ν'^{s})

$$\mathcal{L}_Y = -\sqrt{2}\sum_{\alpha,\beta} Y'_{\alpha\beta}\overline{\psi'^{d}_{\alpha}}\tilde{H}(\nu'^{s}_{\beta})^{c} + \text{h.c.}\,, \tag{1}$$

where α, β run over the flavor indices e, μ, τ. These dimension-4 terms are explicitly invariant under $SU(2) \times U(1)_Y$ for neutrinos and are fully renormalizable, in contrast to higher-dimensional effective operators. In fact, since both the neutrino singlet and its CP conjugate carry no weak isospin or hypercharge ($I = 0, Y = 0$), substituting $(\nu'^{s})^{c}$ for ν'^{s} preserves the gauge invariance of the overall Lagrangian, exactly as in the standard Dirac Yukawa coupling. After spontaneous electroweak symmetry breaking, we obtain

$$\mathcal{L}_Y = -v\sum_{\alpha,\beta} Y_{\alpha\beta}\overline{\nu^{d}_{\alpha}}(\nu^{s}_{\beta})^{c} + \text{h.c.}\,, \tag{2}$$

where $v \approx 246$ GeV is the Higgs vacuum expectation value (VEV). Here, we have transformed the arbitrary basis into the flavor basis. Within the Standard Model (SM) [24], the Yukawa Lagrangian $\mathcal{L}_Y$ in Eq. (2) strictly vanishes (SM) due to chirality and Lorentz invariance constraints ($\overline{\nu_L}\nu_R^{c} = 0$), resulting in massless neutrinos. To generate nonzero mass terms, we minimally extend the SM by introducing a small geometric misalignment between the gauge eigenstates, i.e. the doublet component and singlet, and the chiral eigenstates [1]. The generalized misalignment transformation involves a 6×6 unitary rotation matrix V relating the gauge basis $\Psi_{\text{gauge}} = (\nu^{d}, \nu^{s})^{\mathrm{T}}$ to the chiral basis $\Psi_{\text{chiral}} = (\nu_L, \nu_R)^{\mathrm{T}}$ as follows

$$\begin{pmatrix}\nu^{d}\\ \nu^{s}\end{pmatrix} = V\begin{pmatrix}\nu_L\\ \nu_R\end{pmatrix} = \begin{pmatrix}C_{\mathbf{\Theta}} & S_{\mathbf{\Theta}}\\ -S^{\dagger}_{\mathbf{\Theta}} & \tilde{C}_{\mathbf{\Theta}}\end{pmatrix}\begin{pmatrix}\nu_L\\ \nu_R\end{pmatrix}\,, \tag{3}$$

and

$$\begin{pmatrix}\nu_L\\ \nu_R\end{pmatrix} = V^{\dagger}\begin{pmatrix}\nu^{d}\\ \nu^{s}\end{pmatrix} = \begin{pmatrix}C^{\dagger}_{\mathbf{\Theta}} & -S_{\mathbf{\Theta}}\\ S^{\dagger}_{\mathbf{\Theta}} & \tilde{C}^{\dagger}_{\mathbf{\Theta}}\end{pmatrix}\begin{pmatrix}\nu^{d}\\ \nu^{s}\end{pmatrix}\,, \tag{4}$$

where $C_{\mathbf{\Theta}}$, $S_{\mathbf{\Theta}}$, and $\tilde{C}_{\mathbf{\Theta}}$ are 3×3 complex matrices. The complex misalignment matrix $\mathbf{\Theta}$ serves as the fundamental misalignment parameter that encodes the non-universal flavor structure and CP-violating phases. In the present context, non-universal means that the geometric misalignment is

not identical across the three lepton generations and thus naturally accommodates cross-generational mixing, representing a significant extension to our original work. The non-universal geometry is essentially determined by the unitary matrix V, which imposes the following unitarity requirements to ensure that the proposed gauge-chiral transformation is probability-preserving

$$C_{\mathbf{\Theta}} C_{\mathbf{\Theta}}^{\dagger} + S_{\mathbf{\Theta}} S_{\mathbf{\Theta}}^{\dagger} = I \ , \quad C_{\mathbf{\Theta}} S_{\mathbf{\Theta}} = S_{\mathbf{\Theta}} \tilde{C}_{\mathbf{\Theta}}^{\dagger} \ . \tag{5}$$

In the limit of small misalignment parameters ($|\mathbf{\Theta}_{ij}| \ll 1$), we have

$$S_{\mathbf{\Theta}} \approx \mathbf{\Theta} \ , \tag{6}$$

$$C_{\mathbf{\Theta}} \approx I - \frac{1}{2} \mathbf{\Theta} \mathbf{\Theta}^{\dagger} \ , \tag{7}$$

$$\tilde{C}_{\mathbf{\Theta}} \approx I - \frac{1}{2} \mathbf{\Theta}^{\dagger} \mathbf{\Theta} \ . \tag{8}$$

Note that $\mathbf{\Theta}$ does not generally commute with its Hermitian conjugate ($\mathbf{\Theta}\mathbf{\Theta}^{\dagger} \neq \mathbf{\Theta}^{\dagger}\mathbf{\Theta}$), since it incorporates asymmetric CP-violating phases. As a result, the doublet-LH projection matrix $C_{\mathbf{\Theta}}$ and the singlet-RH projection matrix $\tilde{C}_{\mathbf{\Theta}}$ must be defined independently to fulfill the unitarity requirement in the entire 6×6 space. For small angles ($|\mathbf{\Theta}_{ij}| \ll 1$), the above Taylor expansion provides the second-order corrections for our framework, while preserving the general and non-Hermitian nature of the flavor projection.

Applying 't Hooft's criterion [9], we find that the small misalignment parameter $\mathbf{\Theta}$ is technically natural, because in the limit of $\mathbf{\Theta} \to 0$ ($V \to I$), the RGM model reduces to the exact SM where the neutrino chiral fields perfectly align with the $SU(2)$ representations, leading to massless neutrinos and thus the restoration of the lepton number symmetry.

To describe the deviation from standard three-flavor unitarity, we define the non-unitarity parameter η as

$$\eta = -\frac{1}{2} \mathbf{\Theta} \mathbf{\Theta}^{\dagger} \ , \tag{9}$$

which is Hermitian by construction. The doublet-LH projection block can thus be expressed as $C_{\mathbf{\Theta}} \approx I + \eta$. As will be shown in section 3.1, η gives rise to non-unitary mixing in the active sector.

To clarify how the generalized geometric misalignment is physically structured, we perform a block-wise decomposition of the unitary transformation matrix as illustrated in Fig. 1. By block-partitioning the entire 6×6 matrix $V^{\dagger}$ into four sectors, we identify the following sub-blocks that constitute the mixing:

1. The active sector (top left): The non-unitary portion of this sector determines the observed flavor transitions and is the focus of the precision electroweak constraints that will be explored later in this paper.

2. The misalignment bridge (off-diagonal): These sub-blocks describe the connection between the active and sterile sectors and determine the geometric source of the light Majorana masses.

3. The sterile sector (bottom right): This subspace enforces the unitarity of the full 6×6 matrix by compensating the leakage of probability from the active sector.

$$V^\dagger = \left(\begin{array}{c|c} C_{\mathbf{\Theta}}^\dagger & -S_{\mathbf{\Theta}} \\ \hline S_{\mathbf{\Theta}}^\dagger & \tilde{C}_{\mathbf{\Theta}}^\dagger \end{array}\right) \approx \left(\begin{array}{ccc|ccc} 1+\eta_{ee} & \eta_{\mu e} & \eta_{\tau e} & -\mathbf{\Theta}_{ee} & -\mathbf{\Theta}_{e\mu} & -\mathbf{\Theta}_{e\tau} \\ \eta_{e\mu} & 1+\eta_{\mu\mu} & \eta_{\tau\mu} & -\mathbf{\Theta}_{\mu e} & -\mathbf{\Theta}_{\mu\mu} & -\mathbf{\Theta}_{\mu\tau} \\ \eta_{e\tau} & \eta_{\mu\tau} & 1+\eta_{\tau\tau} & -\mathbf{\Theta}_{\tau e} & -\mathbf{\Theta}_{\tau\mu} & -\mathbf{\Theta}_{\tau\tau} \\ \hline \mathbf{\Theta}_{ee}^* & \mathbf{\Theta}_{\mu e}^* & \mathbf{\Theta}_{\tau e}^* & 1+\tilde{\eta}_{ee} & \tilde{\eta}_{\mu e} & \tilde{\eta}_{\tau e} \\ \mathbf{\Theta}_{e\mu}^* & \mathbf{\Theta}_{\mu\mu}^* & \mathbf{\Theta}_{\tau\mu}^* & \tilde{\eta}_{e\mu} & 1+\tilde{\eta}_{\mu\mu} & \tilde{\eta}_{\tau\mu} \\ \mathbf{\Theta}_{e\tau}^* & \mathbf{\Theta}_{\mu\tau}^* & \mathbf{\Theta}_{\tau\tau}^* & \tilde{\eta}_{e\tau} & \tilde{\eta}_{\mu\tau} & 1+\tilde{\eta}_{\tau\tau} \end{array}\right)$$

Figure 1: The 6×6 unitary misalignment matrix split into sectors to show the flavor state combinations. The top-left 6×6 block $C_{\mathbf{\Theta}}^\dagger \approx I + \eta^\dagger = I + \eta$ shows the visible doublet projection. The off-diagonal block $-S_{\mathbf{\Theta}} \approx -\mathbf{\Theta}$ indicates the invisible singlet fractions contained within the active states. Due to the non-commutative nature from the CP-violating phases, the non-unitary deviation within the sterile sector is described by a distinct parameter, $\tilde{\eta} = -\frac{1}{2}\mathbf{\Theta}^\dagger\mathbf{\Theta}$.

Given this geometric misalignment structure, the active neutrino gauge doublet component ν^d no longer coincides strictly with the LH chiral field ν_L, but instead emerge as a linear superposition of both ν_L and ν_R

$$\nu^d = C_{\mathbf{\Theta}}\nu_L + S_{\mathbf{\Theta}}\nu_R \approx (I+\eta)\nu_L + \mathbf{\Theta}\nu_R \,. \tag{10}$$

Similarly, the invisible gauge singlet ν^s consists predominantly of the RH chiral field ν_R alongside a small fraction of the LH field ν_L

$$\nu^s = -S_{\mathbf{\Theta}}^\dagger\nu_L + \tilde{C}_{\mathbf{\Theta}}\nu_R \approx -\mathbf{\Theta}^\dagger\nu_L + (I+\tilde{\eta})\nu_R \,. \tag{11}$$

Consequently, while the neutrino gauge eigenstates possess well-defined electroweak quantum numbers ($I_3 = 1/2, Y = -1$ for doublet components, $I_3 = 0, Y = 0$ for singlets), the physical neutrinos ν_L and ν_R do not carry these definite quantum numbers due to the geometric misalignment introduced in the present RGM framework. Because weak interactions are constructed strictly by means of gauge-invariant couplings to the $SU(2)$ doublet alone, this framework subtly deviates from the maximal parity violation of the V-A theory established by Wu's experiment [25, 26, 27, 28]. Nevertheless, as the physical ν_R state only acquires a minuscule weak coupling through its tiny doublet fraction, the RH neutrino contribution to weak interactions is actually very small, making it undetectable in the experiments conducted.

2.2 Mass Generation Mechanism

The Majorana neutrino masses naturally emerge after we substitute the rotated gauge fields (Eq. (3)) into the Lagrangian of Eq. (2). The LH and RH fields decouple entirely in the mass terms, as strict chirality and Lorentz invariance constraints ($\overline{\nu_L}\nu_R^c = 0$) force all cross terms to vanish [1]. Hence, LH and RH neutrinos can be treated as independent wave packets during their propagation and detection, enabling us to directly study the non-unitary effects within the active sector in the subsequent sections. Through a straightforward algebraic expansion to first order in $\mathbf{\Theta}$, the symmetric Majorana neutrino mass matrix M_ν [29] in the flavor basis is obtained as

$$M_\nu \approx -v(\mathbf{\Theta}Y^T + Y\mathbf{\Theta}^T) \, . \tag{12}$$

This mass matrix manifests as an anti-commutator of the non-universal misalignment matrix $\mathbf{\Theta}$ and the Yukawa matrix Y, representing a key theoretical result of the RGM framework.

Eq. (12) provides a solution to the long-standing fine-tuning problem associated with Yukawa couplings. In the SM, a typical Dirac term is insufficient to generate a sub-eV neutrino mass unless the Yukawa coupling Y is set to be $\sim 10^{-13} - 10^{-12}$ that is unreasonably small relative to those of charged fermions. However, within the context of our framework, the mass is naturally suppressed by the smallness of the misalignment parameters $|\mathbf{\Theta}_{ij}| \ll 1$. For instance, when $|\mathbf{\Theta}| \sim 10^{-7}$, the desired mass scale $m_\nu \sim 0.05$ eV can be generated with $Y \sim 10^{-6}$, a scale comparable to that of electron. Therefore, a theoretically consistent justification is provided for the tiny neutrino mass without invoking extreme numerical fine-tuning.

Furthermore, the matrix structure of $\mathbf{\Theta}$ allows the neutrino mass hierarchy to be inherited from the misalignment geometry. This means that the experimentally observed mass differences Δm^2_{21} and Δm^2_{31} could reflect the intrinsic flavor dependency of the misalignment of the $SU(2)$ representation space and chiral fields, rather than being a result from some arbitrary construction in the Yukawa sector.

Having developed a geometry-based mechanism for neutrino mass, we will proceed to investigate the phenomenological implications arising from the geometric misalignment characterized by $\mathbf{\Theta}$. As we demonstrate in the subsequent sections, the unique geometry induced by $\mathbf{\Theta}$ leads to the non-unitary mixing within the active sector. This non-unitarity manifests as potential observables including zero-distance flavor transitions, charged lepton flavor violating (cLFV) decays and universality violations in W decays. These signatures offers a path to probe the geometric mechanism behind the electroweak-scale neutrino mass.

3 Non-Unitary Mixing and the Zero-Distance Effect

3.1 Theoretical Probability at $L = 0$

As indicated in section 2.2, the LH and RH neutrino chiral fields are decoupled from each other due to strict chirality and Lorentz invariance constraints. Furthermore, the RH neutrinos constitute a phenomenologically negligible fraction of the initial neutrino flux, as the production of them from weak interactions is geometrically suppressed by a factor of $|\mathbf{\Theta}|^2$ (Eq. (10)). Therefore, we can focus exclusively on the propagation and detection of the active LH neutrino beam. From Eq. (4), the LH chiral field is expressed as a superposition of the gauge doublet component and singlet

$$\nu_L = C_{\mathbf{\Theta}}^{\dagger}\nu^d - S_{\mathbf{\Theta}}\nu^s \ . \tag{13}$$

Given that $|\mathbf{\Theta}_{ij}| \ll 1$ and the singlet ν^s is invisible in weak interactions, the contribution from the second term $S_{\mathbf{\Theta}}\nu^s$ can be safely neglected. Thus, we have

$$\nu_L \approx C_{\mathbf{\Theta}}^{\dagger}\nu^d \approx \left(I - \frac{1}{2}\mathbf{\Theta}\mathbf{\Theta}^{\dagger}\right)\nu^d \ . \tag{14}$$

Inverting the relation in Eq. (14) gives

$$\nu^d \approx \left(I + \frac{1}{2}\mathbf{\Theta}\mathbf{\Theta}^{\dagger}\right)\nu_L = (I - \eta)\nu_L \ . \tag{15}$$

It is apparent that the mixing matrix $(I - \eta)$ is explicitly non-unitary.

In the present framework, the flavor eigenstates $|\nu_\alpha\rangle$ participating in weak interactions are identified as the $SU(2)$ doublet components ν^d. Accordingly, following Eq. (15), we can expand the flavor eigenstates in terms of the mass eigenstates as

$$|\nu_\alpha\rangle \approx (I - \eta)\nu_L = \sum_{i=1}^{3} N_{\alpha i}|\nu_{i,L}\rangle \ , \tag{16}$$

where $N \approx (I-\eta)U_{\rm PMNS}$ is the non-unitary mixing matrix, $U_{\rm PMNS}$ is the unitary PMNS (Pontecorvo-Maki-Nakagawa-Sakata) matrix [29] and $|\nu_{i,L}\rangle$ are the mass eigenstates for the LH neutrinos. The deviation of the active sector from unitarity is thus governed by the misalignment geometry

$$NN^{\dagger} \approx I - 2\eta = I + \mathbf{\Theta}\mathbf{\Theta}^{\dagger} \ . \tag{17}$$

After being normalized by the non-unitary factors associated with the active subspace, the physical transition probability $P_{\alpha\beta}(L)$ reads [30]

$$P_{\alpha\beta}(L) = \frac{|\sum_{i=1}^{3} N_{\alpha i}N_{\beta i}^{*}\exp(-i\frac{m_i^2 L}{2E})|^2}{(NN^{\dagger})_{\alpha\alpha}(NN^{\dagger})_{\beta\beta}} \ , \tag{18}$$

where the exponential terms become unity for $L \to 0$. Substituting Eq. (17) into Eq. (18), we obtain the zero-distance flavor transition probability

$$P_{\alpha\beta}(0) \approx \frac{|(NN^\dagger)_{\alpha\beta}|^2}{(NN^\dagger)_{\alpha\alpha}(NN^\dagger)_{\beta\beta}} \approx |(\boldsymbol{\Theta}\boldsymbol{\Theta}^\dagger)_{\alpha\beta}|^2 \quad (\alpha \neq \beta) \,. \tag{19}$$

Eq. (19) demonstrates that the misalignment, characterized by $\boldsymbol{\Theta}$, induces an instantaneous flavor change at the source. This is equivalent to an oscillation averaged over very large mass-squared splittings $\Delta m^2 \to \infty$, resulting in a flat excess of events which is independent of energy E or baseline L in the experiment. Regarding the diagonal effect, the total observed active flux is slightly suppressed by the factor $(C_{\boldsymbol{\Theta}} C_{\boldsymbol{\Theta}}^\dagger)^2_{\alpha\alpha} \approx 1+4\eta_{\alpha\alpha}$ (which equals $1-2(\boldsymbol{\Theta}\boldsymbol{\Theta}^\dagger)_{\alpha\alpha}$). Our RGM model thus offers a purely geometric origin for the short-baseline (SBL) anomalies, distinct from the effect of L/E-dependent oscillations in standard theories.

3.2 Numerical Analysis of LSND/MiniBooNE and MicroBooNE

The SBL LSND and MiniBooNE anomalies report a surplus of electron-like events detected in muon-flavor neutrino beams. By scaling the total excess of electron-like events to the total neutrino flux, we obtain an effective phenomenological transition probability $P_{\mu e}(L) \sim 2.0 \times 10^{-3}$ [15, 16, 17, 18]. Unlike the conventional 3+1 sterile-neutrino framework [31, 32, 33, 34] that relies on an eV-scale mass splitting to drive the L/E-dependent oscillations, the RH states in our model are mass-degenerate and chirally decoupled from the active LH neutrinos. Therefore, within the present context, the anomalies can only be explained by the instantaneous, non-unitary flavor change that takes place at the source. This means $P_{\mu e}(0) \sim 2.0 \times 10^{-3}$, which requires

$$|(\boldsymbol{\Theta}\boldsymbol{\Theta}^\dagger)_{\mu e}|^2 \approx 2 \times 10^{-3} \implies |(\boldsymbol{\Theta}\boldsymbol{\Theta}^\dagger)_{\mu e}| \approx 0.045 \,. \tag{20}$$

To produce a product of off-diagonal mixing of this size, the individual entries in the generalized misalignment matrix would typically be around $|\boldsymbol{\Theta}| \sim \sqrt{0.045} \approx 0.2$.

The LSND and MiniBooNE anomalies have been traditionally explained by oscillations involving at least one light sterile neutrino [31, 32, 33, 34]. However, the 2025 MicroBooNE collaboration has excluded the single light sterile neutrino interpretation at the 95% CL [10], by utilizing both the Booster Neutrino Beam (BNB) and the Neutrinos at the Main Injector (NuMI) beam. Importantly, MicroBooNE found no evidence for an excess of electron neutrino events consistent with standard L/E-dependent $\nu_\mu \to \nu_e$ oscillations, thereby ruling out the simple 3+1 sterile-neutrino hypothesis.

While the RGM model can explain the observed LSND and MiniBooNE anomalies solely through non-unitarity with a misalignment of $|\boldsymbol{\Theta}| \sim 0.2$, the Yukawa coupling has to be significantly suppressed. In fact, from the mass generation Eq. (12), we find

$$Y \sim \frac{m_\nu}{2|\boldsymbol{\Theta}|v} = \frac{0.05 \text{ eV}}{2(0.2)(246 \text{ GeV})} \sim 5 \times 10^{-13} \,, \tag{21}$$

for $m_\nu \sim 0.05$ eV. This again introduces the fine-tuning issue. Since the main objective of our RGM framework is to enable natural, electron-like Yukawa couplings with a highly suppressed misalignment scale, we thereby classify the parameter space into three different regimes for further investigation:

1. Natural regime ($|\mathbf{\Theta}| \sim 10^{-7}$, $Y \sim 10^{-6}$) [1]: Explains the mass naturally with electron-like Yukawa couplings, yet predicts zero observable SBL effects.

2. High-mixing regime ($|\mathbf{\Theta}| \sim 10^{-1}$, $Y \sim 10^{-12}$): Explains the SBL anomalies via the zero-distance non-unitary effect, but introduces the fine tuning problem as shown in Eq. (21).

3. Intermediate regime ($|\mathbf{\Theta}| \sim 10^{-3} - 10^{-2}$, $Y \sim 10^{-10}$): Safely satisfies the MicroBooNE null result while retaining a sufficiently large non-unitarity parameter to provide observable signatures at future high-precision facilities.

Note that in the MicroBooNE ν_e spectrum, a transition probability $P_{\mu e}(0)$ exceeding approximately 10^{-3} would have manifested as a discernible normalization shift. To first order, this gives

$$P_{\mu e}(0) \approx |(\mathbf{\Theta}\mathbf{\Theta}^\dagger)_{\mu e}|^2 \leq 10^{-3} \implies |(\mathbf{\Theta}\mathbf{\Theta}^\dagger)_{\mu e}| \leq 0.03 \,. \tag{22}$$

Clearly, the natural regime is entirely compatible with this MicroBooNE limit. Within this regime, a misalignment scale of $|\mathbf{\Theta}| \sim 10^{-7}$ produces the observed neutrino mass scale of $m_\nu \sim 0.05$ eV with electron-like Yukawa couplings of $Y \sim 10^{-6}$, and predicts a zero-distance effect of $P_{\mu e}(0) \sim 10^{-28}$ that is equivalent to zero for practical experiments. Between the MicroBooNE-excluded high-mixing regime and the natural regime, however, there could exist an intermediate regime ($|\mathbf{\Theta}| \sim 10^{-3} - 10^{-2}$). With a moderate suppression of the Yukawa coupling ($Y \sim 10^{-10}$), this parameter space satisfies the MicroBooNE null result while retaining a sufficiently large non-unitarity parameter to provide observable signatures for future precision experiments. The relationship between the misalignment scale $|\mathbf{\Theta}|$, the required Yukawa coupling, and the boundaries of the distinct phenomenological regimes is visually summarized in Fig. 2 and will be further discussed in the next section.

4 Constraints from Precision Physics

In the preceding section, we utilizes the LSND and MiniBooNE anomalies along with the MicroBooNE null result to constrain the off-diagonal element $|(\mathbf{\Theta}\mathbf{\Theta}^\dagger)_{\mu e}|$ via the zero distance $\nu_\mu \to \nu_e$ and $\bar{\nu}_\mu \to \bar{\nu}_e$ flavor transitions. However, precision physics provides stronger constraints on the broader non-unitary parameters. In this section, we evaluate these limits by using two primary probes: charged lepton flavor violating (cLFV) decays [12, 13, 30, 35, 36, 37] and lepton universality tests in W-boson decays [14, 38, 39].

4.1 Radiative Decay ($\mu \to e\gamma$)

The non-unitarity of the neutrino mixing matrix N leads to unique characteristics in cLFV decays, particularly the radiative decay $\mu \to e\gamma$. In standard high-scale seesaw scenarios, this radiative transition is mediated by quantum loops involving the W boson and light neutrinos. The rate of the process therein is suppressed due to the unitarity of the mixing matrix and the smallness of the neutrino masses compared to the mass of the W boson [40, 41]. The result is an experimentally undetectable rate ($\mathcal{B} \sim 10^{-54}$) [35]. In the present misalignment framework, however, the active mixing matrix N is a non-unitary sub-block of a larger unitary matrix 6×6, with the non-orthogonality of the flavor states demonstrated as follows

$$\sum_{i=1}^{3} N_{\mu i} N_{ei}^{*} = (NN^{\dagger})_{\mu e} \approx (\boldsymbol{\Theta}\boldsymbol{\Theta}^{\dagger})_{\mu e} \, . \tag{23}$$

Further, since the mass-degenerate RH neutrinos are decoupled from the LH neutrinos in the present framework, there is no interference that can restore unitarity in the loop. Thus, the branching ratio can be expressed in the form of [30, 36]

$$\mathcal{B}(\mu \to e\gamma) \approx \frac{100\alpha}{96\pi} |(\boldsymbol{\Theta}\boldsymbol{\Theta}^{\dagger})_{\mu e}|^2 \, , \tag{24}$$

where $\alpha \approx 1/137$ is the fine structure constant. Applying the July 2025 data of the MEG II collaboration [12]

$$\mathcal{B}(\mu^{+} \to e^{+}\gamma) < 1.5 \times 10^{-13} \quad (90\% \text{ C.L.}) \, , \tag{25}$$

we find

$$|(\boldsymbol{\Theta}\boldsymbol{\Theta}^{\dagger})_{\mu e}| \leq 7.9 \times 10^{-6} \, , \tag{26}$$

which is approximately four orders of magnitude tighter compared to the zero-distance transition bounds, i.e., 0.045 and 0.03, derived from LSND/MiniBooNE and MicroBooNE results (Eq. (20) and (22)) respectively.

This stringent constraint from MEG II has significant implications for the misalignment parameter space. In the high-mixing regime ($|\boldsymbol{\Theta}| \sim 10^{-1}$), the predicted branching ratio exceeds the experimental MEG II limit by many orders of magnitude and is therefore phenomenologically excluded. On the other hand, the off-diagonal mixing element in the natural regime ($|\boldsymbol{\Theta}| \sim 10^{-7}$) is highly suppressed such that $|(\boldsymbol{\Theta}\boldsymbol{\Theta}^{\dagger})_{\mu e}| \sim 10^{-14}$, yielding a vanishing branching ratio of $\mathcal{B}(\mu \to e\gamma) \sim 10^{-31}$ which falls far below any current or planned detection thresholds.

4.2 Universality Tests in W Decays

The non-unitarity of the mixing matrix N has profound implications for electroweak precision observables, primarily due to the modification of the Fermi constant [30, 42]. In the SM, the Fermi

constant G_F is extracted from the muon lifetime under the assumption of unitary lepton mixing [38]. However, in the presence of non-unitarity, the experimentally extracted value G_μ is different from the fundamental combination of the gauge coupling g and the mass of the W-boson M_W. Explicitly, the measured value is modified by the diagonal non-unitarity parameters [30]:

$$G_\mu \approx G_F(1 - \eta_{ee} - \eta_{\mu\mu}) \,, \tag{27}$$

where G_F denotes the Fermi constant in the absence of non-unitarity [38]. This modification alters the partial decay width of the W boson to a lepton and its neutrino, $W \to l\nu_l$. A sensitive test of such an effect is the ratio of the two decay widths, which is used as a probe of lepton-flavor universality. Using the derivation in Ref. [42], we have the simplified linear form for the ratio

$$R^W_{\mu/e} = \frac{\mathcal{B}(W \to \mu\nu)}{\mathcal{B}(W \to e\nu)} \approx 1 + 2(\eta_{ee} - \eta_{\mu\mu}) \,. \tag{28}$$

Based on 140 fb^{-1} of pp collision data, the ATLAS measurement of 2024 has reported $R^W_{\mu/e} = 0.9995 \pm 0.0045$ [14], with significantly reduced uncertainty . This result is consistent with the 2024 PDG global fit [38] and provides a stringent constraint on the deviation from universality as follows

$$|R^W_{\mu/e} - 1| \lesssim 0.0050 \,, \tag{29}$$

which imposes a constraint on the absolute difference between the diagonal non-unitary parameters. Using $\eta = -\frac{1}{2}\boldsymbol{\Theta}\boldsymbol{\Theta}^\dagger$ (Eq. (9)), the above bound translates directly to

$$|(\boldsymbol{\Theta}\boldsymbol{\Theta}^\dagger)_{ee} - (\boldsymbol{\Theta}\boldsymbol{\Theta}^\dagger)_{\mu\mu}| < 0.0050 \,. \tag{30}$$

Note that this diagonal ATLAS bound is positioned just between the two extremes of off-diagonal limits: the tight MEG II constraint on the off-diagonal cross-mixing ($\sim 10^{-6}$) and the relatively weaker bounds derived from the zero-distance flavor transitions of LSND/MiniBooNE (0.045) and MicroBooNE (0.03).

For the high-mixing regime ($|\boldsymbol{\Theta}| \sim 10^{-1}$) where the off-diagonal element is sufficiently large to account for the SBL anomalies ($|(\boldsymbol{\Theta}\boldsymbol{\Theta}^\dagger)_{\mu e}| \approx 0.045$), this ATLAS constraint is difficult to be satisfied. In this scenario, the corresponding diagonal entries could also be comparably large. Thus, their absolute difference would exceed the above ATLAS universality bound, unless the diagonal elements are artificially fine-tuned to a precision of $\mathcal{O}(10^{-3})$. On the other hand, the natural regime ($|\boldsymbol{\Theta}| \sim 10^{-7}$) predicts ultra-suppressed diagonal elements of $|(\boldsymbol{\Theta}\boldsymbol{\Theta}^\dagger)_{\alpha\alpha}| \sim 10^{-14}$. This scale eliminates the difference between the electron and muon sectors and satisfies the lepton flavor universality requirements by more than eleven orders of magnitude.

Fig. 2 shows a rigorous comparison of the present framework with both the electroweak precision tests and the SBL neutrino constraints. The shaded-red exclusion region establishes the hard upper

limit for low-scale mass generation through the combination of the MEG II radiative decay bound and the ATLAS W-decay universality measurement. Note that MEG II strictly limits the off-diagonal cross mixing ($|\mathbf{\Theta}_{\mu e}| \lesssim 2.8 \times 10^{-3}$) while ATLAS bounds the diagonal elements ($|\mathbf{\Theta}_{\alpha\alpha}| \lesssim 7.1 \times 10^{-2}$). Thus, the precise boundaries of the misalignment parameter space are actually flavor-dependent. As shown in the figure, the high-mixing regime appears to be excluded, whereas the natural regime, representing full technical naturalness of the RGM model, is located well below all experimental thresholds. Between the established bounds and the natural regime is the intermediate regime ($|\mathbf{\Theta}| \sim 10^{-3} - 10^{-2}$). In this space, an appropriate flavor structure will evade the stringent MEG II limit through a sufficiently suppressed off-diagonal sector, while allowing the diagonal non-unitarity to remain large enough ($|\eta_{\alpha\alpha}| \sim 10^{-5} - 10^{-4}$) to provide observable signatures at high-precision neutrino facilities such as DUNE and Hyper-K.

5 Radiative Stability and Naturalness

We will now test the technically natural scenario by examining the radiative corrections to the non-unitarity parameter, $\eta = -\frac{1}{2}\mathbf{\Theta}\mathbf{\Theta}^\dagger$. In high-scale Type-I seesaw models, heavy Majorana neutrino loops generate radiative corrections to the Higgs mass parameter that are quadratically sensitive to the heavy neutrino mass scale, potentially leading to an electroweak naturalness problem [6, 43, 44, 45]. However, in the low-scale RGM framework, the smallness of the misalignment is protected by 't Hooft's naturalness criterion [9], since in the limit of $\mathbf{\Theta} \to 0$ or $\eta \to 0$, the $SU(2)$ representation space is completely aligned with the chiral fields, yielding massless neutrinos and thus the restoration of lepton number symmetry.

To verify this stability, we analyze the one-loop renormalization group equation (RGE) for the non-unitarity parameter η [7, 46, 47, 48]. Following standard procedures, the evolution is derived from the wave-function renormalization of the lepton doublets and singlets within the interaction Lagrangian Eq. (1). Utilizing the product rule on the definition of η, the RGE is found to be

$$16\pi^2 \frac{d\eta}{d\ln\mu} \approx C_1(YY^\dagger)\eta + C_2\eta(YY^\dagger) + \dots\,, \tag{31}$$

where μ represents the renormalization scale, $16\pi^2$ is the standard one-loop factor, and Y represents the neutrino Yukawa matrix.

As demonstrated in Eq. (31), the beta function has a multiplicative form, ensuring that $\eta = 0$ is a fixed point of the RGE flow. A small value of the non-unitarity parameter, either 10^{-14} in the natural regime or 10^{-2} in the high-mixing regime, therefore does not receive large additive corrections from higher energy scales. In the natural regime with $|\eta| \sim 10^{-14}$, the framework generates the neutrino mass scale $m_\nu \sim 0.05$ eV with natural, electron-like Yukawa couplings $Y \sim 10^{-6}$ [1]. This radiatively

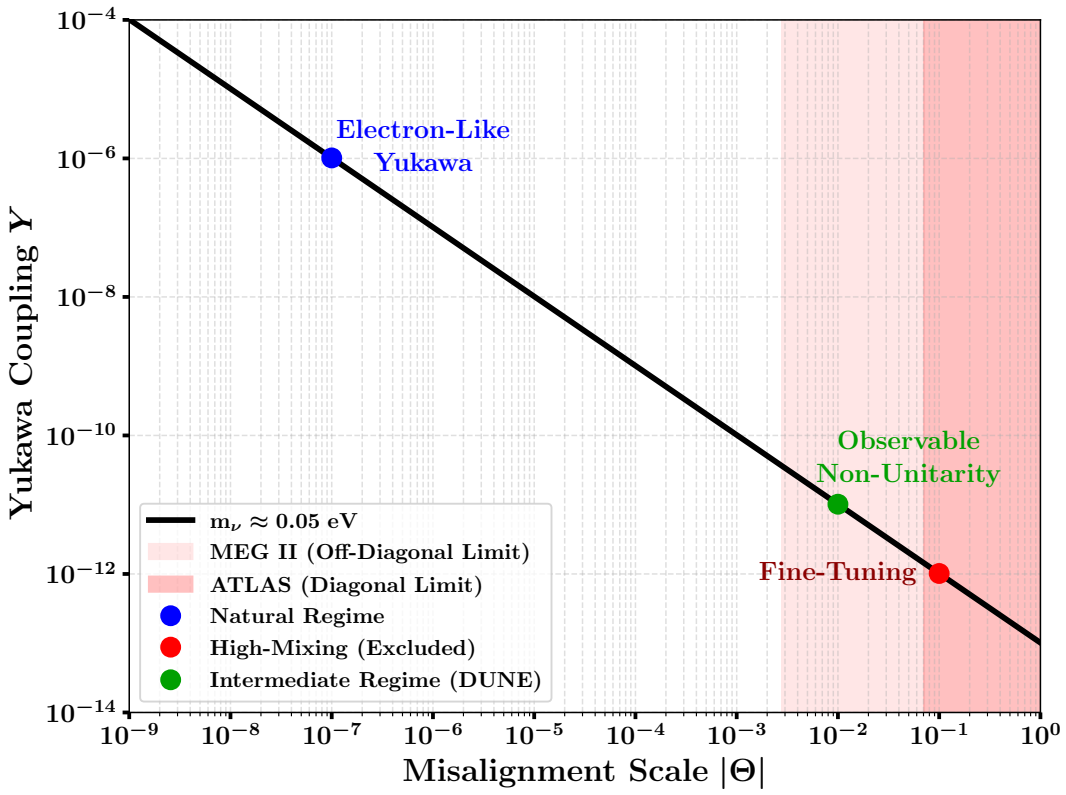


Figure 2: Parameter space of the generalized geometric misalignment framework. The diagonal black line corresponds to the constant product $|\boldsymbol{\Theta}|Y$ required to generate a Majorana neutrino mass of $m_\nu \approx 0.05$ eV (Eq. (12)). The red shaded regions denote the parameter space constrained by precision electroweak bounds. The solid-red exclusion zone begins at $|\boldsymbol{\Theta}| \approx 7.1 \times 10^{-2}$, representing the ATLAS W-decay universality limits on the diagonal elements. The extended light-red region is further bounded by the tighter MEG II limit on the off-diagonal cross-mixing ($|\boldsymbol{\Theta}_{\mu e}| \lesssim 2.8 \times 10^{-3}$). Within this space, the intermediate regime could be detectable, provided the off-diagonal components are sufficiently suppressed.

stable approach effectively solves the persistent fine-tuning problem encountered in the standard Dirac or high-scale seesaw models. Moreover, the stability of η ensures that the resulting non-unitary effects are not destroyed by loop corrections. This gives our geometric mass model a strong predictive power for future LBL experiments.

6 Implications for the Precision Frontier: DUNE and Hyper-K

It has been shown in the prior sections that the geometric misalignment framework is constrained by current precision data and protected by radiative stability. In this section, we will study the experimental testability of the geometric misalignment, whose observable effects are determined by the non-unitarity parameter $\eta = -\frac{1}{2}\boldsymbol{\Theta}\boldsymbol{\Theta}^\dagger$. It was found that at the microscopically small scale of the natural regime $|\boldsymbol{\Theta}| \sim 10^{-7}$, the off-diagonal flavor transitions ($|\eta|^2 \sim 10^{-28}$) and the diagonal electroweak precision corrections ($\eta \sim 10^{-14}$) are well below the experimental sensitivity limits. Thus, in this scenario, the RGM framework cannot be distinguished from standard unitary mixing at current and next-generation facilities, since the non-unitary effects induced by the proposed geometry are obscured by the standard oscillation signals.

Considering the experimentally accessible regions of the parameter space, we have identified an intermediate regime that satisfies the current constraints but within the reach of upcoming experiments. As noted in section 4, the precise boundaries of the excluded parameter space are substantially flavor-dependent. In fact, the recent MEG II limit $\mathcal{B} < 1.5 \times 10^{-13}$ for $\mu^+ \to e^+\gamma$ constrains the off-diagonal cross-mixing to $|(\boldsymbol{\Theta}\boldsymbol{\Theta}^\dagger)_{\mu e}| \leq 7.9 \times 10^{-6}$, corresponding to $|\eta_{\mu e}| \leq 4.0 \times 10^{-6}$. On the other hand, the 2024 ATLAS measurements on the W-decay lepton universality bound the diagonal components to $|(\boldsymbol{\Theta}\boldsymbol{\Theta}^\dagger)_{\alpha\alpha}| \lesssim 5.0 \times 10^{-3}$, which is equivalent to $|\eta_{\alpha\alpha}| \leq 2.5 \times 10^{-3}$. Nature can accommodate an intermediate regime with $|\boldsymbol{\Theta}| \sim 10^{-3} - 10^{-2}$ by constructing a flavor pattern that suppresses the off-diagonal sector by only one order of magnitude more than the diagonal elements to avoid breaking the MEG II bound. With such suppression, the diagonal non-unitary elements could remain large enough ($|\eta_{\alpha\alpha}| \sim 10^{-5} - 10^{-4}$) to place the upper end of this range within the reach of future precision facilities. Although the generation of a 0.05 eV neutrino mass in this intermediate regime will require a Yukawa coupling of $Y \sim 10^{-10}$, it is still about $2-3$ orders of magnitude more natural than the extremely unnatural $Y \sim 10^{-13}$ required by standard Dirac mass models.

By nature, the non-unitary mixing matrix $N \approx (I-\eta)U_{\rm PMNS}$ can introduce additional CP-violating phases absent in the standard three-flavor paradigm. To demonstrate this, we parameterize the $\mu - e$ off-diagonal non-unitarity element as $\eta_{\mu e} = |\eta_{\mu e}|e^{-i\phi_{\mu e}}$, such that we can decompose the oscillation probability for the $\nu_\mu \to \nu_e$ appearance channel into three distinct terms

$$P(\nu_\mu \to \nu_e) \approx P_{\rm SM}(\delta_{\rm CP}) + P_{\rm zero}(|\eta_{\mu e}|) + P_{\rm int}(|\eta_{\mu e}|, \phi_{\mu e}, \delta_{\rm CP}) \,, \tag{32}$$

where $P_{\rm SM}$ is the standard unitary PMNS oscillation governed by the mass-squared splittings and modulated by the standard Dirac CP phase $\delta_{\rm CP}$. The second term, $P_{\rm zero} \approx 4|\eta_{\mu e}|^2$, is the instantaneous zero-distance transition probability. The last term, $P_{\rm int}$, represents the interference between the zero-distance transitions and the standard oscillation amplitudes, and is sensitive to the new geometric CP-violating phase $\phi_{\mu e}$.

Because this geometric phase $\phi_{\mu e}$ can constructively or destructively interfere with standard oscillations, it will induce a shift in the observed effective CP asymmetry. To leading order, the effective CP asymmetry is found to be linearly shifted by an additive geometric perturbation

$$A_{\rm CP}^{\rm eff} \equiv \frac{P(\nu_\mu \to \nu_e) - P(\overline{\nu}_\mu \to \overline{\nu}_e)}{P(\nu_\mu \to \nu_e) + P(\overline{\nu}_\mu \to \overline{\nu}_e)} \approx A_{\rm CP}^{\rm SM}(\delta_{\rm CP}) + \Delta A_{\rm CP}^{\rm geom}(|\eta_{\mu e}|, \phi_{\mu e}, \delta_{\rm CP}) \,, \tag{33}$$

which exhibits a coupled dependence on both the geometric phase and the standard Dirac phase.

However, because the MEG II limit constrains the off-diagonal parameter $|\eta_{\mu e}|$ so tightly, the resulting geometric CP-violating perturbation is heavily suppressed to $\mathcal{O}(10^{-6})$, which is well below the $\mathcal{O}(10^{-2})$ systematic uncertainty threshold of next-generation appearance measurements. Thus, measurements of the standard Dirac phase $\delta_{\rm CP}$ at DUNE and Hyper-K will be untainted by the geometry-induced non-unitarity at least within the highly constrained $\nu_\mu \to \nu_e$ channel. Nevertheless, other flavor transitions, particularly those involving the τ sector, remain open and viable targets for the detection of the corresponding geometric phases.

Therefore, the principal channel for discovering the intermediate regime at future LBL experiments, particularly DUNE [19, 20] and Hyper-K [21, 22, 23], would be based upon the much greater diagonal non-unitarity parameters ($|\eta_{\alpha\alpha}| \approx 10^{-4}$) rather than the geometric CP effects, which are heavily suppressed in the in the primary $\mu - e$ transitions. Notably, this intermediate scale comfortably satisfies the strong limits imposed by the ATLAS W-boson decay universality tests which restrict the diagonal components to $\lesssim 10^{-3}$. Benefiting from the wide-band neutrino beam and high-resolution liquid argon time projection chambers, DUNE will provide precise measurements of the energy-dependent oscillation spectra. Meanwhile, Hyper-K, employing next-generation large water Cherenkov detector, will deliver large statistics for high-precision measurements of neutrino oscillations. Importantly, these facilities can probe the unconstrained parameter space below the ATLAS limit by reaching sensitivities on the order of $\mathcal{O}(10^{-4} - 10^{-3})$. This places the upper limit of the intermediate regime on the sensitivity horizon of these two experiments. A statistically significant deviation from the standard unitary oscillation prediction, manifested as a tension that cannot be resolved between the appearance ($\nu_\mu \to \nu_e$) and disappearance ($\nu_\mu \to \nu_\mu$) channels within the conventional three-neutrino framework, would provide a strong signature of the underlying geometric misalignment. Thus, even though the $\mu - e$ off-diagonal CP-violating effects cannot be observed directly in the appearance channel due to the stringent MEG II constraint, the diagonal effects from the intermediate regime could induce a

significant tension in the standard appearance-disappearance fit.

7 Conclusion

This paper generalizes our recently proposed renormalizable geometric misalignment (RGM) mass model for neutrinos [1] and explores its phenomenological consequences. It is demonstrated that a subtle geometric misalignment between the $SU(2)$ gauge representation space and the chiral fields provides a natural and electroweak origin for the degenerate Majorana neutrino masses which appear to be a linear function of the non-universal misalignment matrix $\mathbf{\Theta}$ (Eq. (12)). This purely geometric mechanism explains the extreme suppression of the neutrino mass scale without invoking heavy new physics or non-renormalizable effective operators. Specifically, a 0.05 eV mass scale can be achieved with electron-like Yukawa couplings ($Y \sim 10^{-6}$), thus resolving the persistent fine-tuning problem inherent in standard Dirac and high-scale seesaw models.

Following 't Hooft's naturalness criterion [9], the smallness of the proposed geometric misalignment is protected by the restoration of lepton number symmetry in the limit of vanishing misalignment. Our analysis on the RGE for the non-unitarity parameter η shows that this symmetry protection prevents η from acquiring divergent loop corrections, and thus ensures its radiative stability over accessible energy scales.

A comprehensive comparison of this framework with the latest 2024–2025 experimental landscape identifies three distinct phenomenological regimes. In the high-mixing regime ($|\mathbf{\Theta}| \sim 10^{-1}$), our framework offers an effective explanation for the LSND and MiniBooNE SBL anomalies [15, 16, 17, 18] through zero-distance flavor transitions. However, this scenario reintroduces the fine-tuning issue and is excluded by the MicroBooNE null result, the $\mu^+ \to e^+\gamma$ decay limit from MEG II [12, 13] and the W-decay universality measurement by ATLAS [14]. Conversely, the highly suppressed natural regime ($|\mathbf{\Theta}| \sim 10^{-7}$) safely satisfies all precision bounds and successfully generates the observed sub-eV mass scale without requiring fine-tuning. Nevertheless, its non-unitary effects are too small for direct observation.

As a bridge between these two extremes, the flavor-dependent intermediate regime with $|\mathbf{\Theta}| \sim 10^{-3} - 10^{-2}$ can represent a practical target for future precision facilities, particularly DUNE [19, 20] and Hyper-K [21, 22, 23]. The flavor structure of this regime sufficiently suppresses the off-diagonal mixing to evade the stringent MEG II bounds, while permitting the diagonal parameters $|\eta_{\alpha\alpha}| \sim 10^{-4}$ that satisfy the ATLAS W-decay universality limit and fall within the reach of the next-generation long-baseline experiments. Accordingly, the primary signature at these facilities would manifest through diagonal non-unitarity. An irreconcilable tension observed between the appearance ($\nu_\mu \to \nu_e$) and disappearance ($\nu_\mu \to \nu_\mu$) channels, when interpreted within the standard unitary framework,

would provide a clear signature of the present geometric misalignment model.

Declarations The author has no competing interests to declare that are relevant to the content of this article.

Data availability As a theoretical work, this study does not generate or use any datasets.

References

[1] W. Wang, Low-scale Majorana neutrino masses from renormalizable Higgs doublet coupling, Eur. Phys. J. Plus **141**, 78 (2026).

[2] P. Minkowski, $\mu \to e\gamma$ at a rate of one out of 10^9 muon decays?, Phys. Lett. B **67**, 421 (1977).

[3] M. Gell-Mann, P. Ramond, R. Slansky, Complex Spinors and Unified Theories, in Supergravity, ed. by F. van Nieuwenhuizen, D. Freedman (North Holland, Amsterdam, 1979).

[4] R.N. Mohapatra, G. Senjanović, Neutrino masses and mixings in gauge models with spontaneous parity violation. Phys. Rev. D **23**, 165 (1981).

[5] S. F. King, Right-handed neutrinos: seesaw models and signatures, arXiv:2502.07877.

[6] F. Vissani, Do experiments suggest a hierarchy problem?, Phys. Rev. D **57**, 7027 (1998).

[7] S. Antusch et al., Running neutrino mass parameters in see-saw scenarios, J. High Energy Phys. **03**, 024 (2005).

[8] A. Ibarra, E. Molinaro, S. T. Petcov. TeV scale see-saw mechanisms of neutrino mass generation, the Majorana nature of the heavy singlet neutrinos and $(\beta\beta)_{0\nu}$-decay, J. High Energy Phys. **09**, 108 (2010).

[9] G. 't Hooft, Naturalness, chiral symmetry, and spontaneous chiral symmetry breaking, NATO Sci. Ser. B **59**, 135 (1980).

[10] P. Abratenko et al. (MicroBooNE Collaboration), Search for Neutrino Oscillations, Nature, **648**, 64 (2025).

[11] P. Abratenko et al. (MicroBooNE Collaboration), Search for an Excess of Electron Neutrino Interactions in MicroBooNE Using Multiple Final-State Topologies, Phys. Rev. Lett. **128**, 241801 (2022).

[12] K. Afanaciev et al. (MEG II Collaboration), New limit on the $\mu^+ \to e^+\gamma$ decay with the MEG II experiment, arXiv:2504.15711 [hep-ex] (2025).

[13] K. Afanaciev, A. M. Baldini, S. Ban et al., A search for $\mu^+ \to e^+\gamma$ with the first dataset of the MEG II experiment. Eur. Phys. J. C **84**, 216 (2024).

[14] G. Aad et al. (ATLAS Collaboration), Precise test of lepton flavour universality in W-boson decays into muons and electrons in pp collisions at $\sqrt{s} = 13$ TeV with the ATLAS detector, Eur. Phys. J. C **84**, 993 (2024).

[15] A. Aguilar et al. (LSND Collaboration),"Evidence for neutrino oscillations from the observation of $\bar{\nu}_e$ appearance in a $\bar{\nu}_\mu$ beam," Phys. Rev. D **64**, 112007 (2001).

[16] C. Athanassopoulos et al. (LSND Collaboration), Phys. Rev. Lett. **77**, 3082 (1996).

[17] A.A. Aguilar-Arevalo et al. (MiniBooNE Collaboration), Updated MiniBooNE neutrino oscillation results with increased data and new background studies, Phys. Rev. D **103**, 052002 (2021).

[18] A.A. Aguilar-Arevalo et al. (MiniBooNE Collaboration), Significant excess of electronlike events in the MiniBooNE short-baseline neutrino experiment, Phys. Rev. Lett. **121**, 221801 (2018).

[19] R. Acciarri et al., Deep Underground Neutrino Experiment (DUNE) far detector technical design report, (2020). B. Abi et al., JINST **15**, T08008 (2020).

[20] Francisco Martínez López for the DUNE collaboration, DUNE: science and status, https://arxiv.org/pdf/2502.08493.

[21] U. Kose, on behalf of Hyper-Kamiokande collaboration, The Hyper-Kamiokande experiment: Status and prospect, SciPost Phys. Proc. **17**, 019 (2025).

[22] Hyper-Kamiokande Collaboration, Sensitivity of the Hyper-Kamiokande experiment to neutrino oscillation parameters using accelerator neutrinos, Eur. Phys. J. C **86**, 170 (2026).

[23] K. Abe et al., Hyper-Kamiokande design report, (arXiv preprint), https://doi.org/10.48550/arXiv.1805.04163.

[24] S.L. Glashow, Partial-symmetries of weak interactions. Nucl. Phys. **22**, 579 (1961).

[25] C. S. Wu et al., Experimental test of parity conservation in beta decay, Phys. Rev. **105**, 1413 (1957).

[26] R. P. Feynman, M. Gell-Mann, Theory of the Fermi interaction, Phys. Rev. **109**, 193 (1958).

[27] E.C.G. Sudarshan, R.E. Marshak, Chirality invariance and the universal Fermi interaction, Physical Review **109**, 1860 (1958).

[28] E. C. G. Sudarshan, R. E. Marshak, Origin of the universal V-A theory, AIP Conference Proceedings **300**, 110 (1994).

[29] S. Bilenky, Introduction to the physics of massive and mixed neutrinos, Lecture notes in physics, 2nd edn. (Spinger, Berlin, 2018).

[30] S. Antusch et al., Unitarity of the leptonic mixing matrix, J. High Energy Phys. **10**, 084 (2006).

[31] K. N. Abazajian et al., Light Sterile Neutrinos: A White Paper, arXiv:1204.5379 (2012).

[32] J. Kopp et al., Sterile neutrino oscillations: the global picture. J. High Energ. Phys. **2013**, 50 (2013). https://doi.org/10.1007/JHEP05(2013)050.

[33] M. Dentler et al., Updated global analysis of neutrino oscillations in the presence of eV-scale sterile neutrinos, J. High Energy Phys. **2018**, 10 (2018).

[34] C. Giunti, T. Lasserre, eV-scale sterile neutrinos, Annu. Rev. Nucl. Part. Sci. **69**, 163 (2019).

[35] L. Calibbi, Charged lepton flavour violation: An experimental and theoretical introduction, Riv. Nuovo Cimento, Vol. **41**, 71 (2018).

[36] S. Antusch, O. Fischer, Non-unitarity of the leptonic mixing matrix: present bounds and future sensitivities, J. High Energy Phys. **10**, 094 (2014).

[37] Y. Kuno, Y. Okada, Muon decay and physics beyond the standard model, Rev. Mod. Phys. **73**, 151 (2001).

[38] S. Navas et al. (Particle Data Group), Phys. Rev. D **110**, 030001 (2024).

[39] LEP Collaborations, Electroweak measurements in electron–positron collisions at W-boson-pair energies at LEP, Phys. Rept. **532**, 119 (2013).

[40] S. T. Petcov, The Processes $\mu \to e + \gamma$, $\mu \to e + e + \bar{e}$, $\nu' \to \nu + \gamma$ in the Weinberg-Salam Model with Neutrino Mixing, Sov. J. Nucl. Phys. **25**, 340 (1977) [Yad. Fiz. 25, 641 (1977)].

[41] B. W. Lee, S. Pakvasa, R. E. Shrock, and H. Sugawara, Muon and electron number nonconservation in a V-A gauge model, Phys. Rev. Lett. **38**, 937 (1977).

[42] Fernandez-Martinez et al., Global constraints on heavy neutrino mixing, JHEP **1608**, 033 (2016).

[43] J. A. Casas et al., Implications for new physics from fine-tuning arguments 1. Application to SUSY and seesaw cases, JHEP **11**, 057 (2004).

[44] A. Abada et al., Low energy effects of neutrino masses, JHEP **0712**, 061 (2007).

[45] G. Bambhaniya et al., Naturalness, vacuum stability, and leptogenesis in the minimal seesaw model, Phys. Rev. D **95**, 095016 (2017).

[46] S. Antusch et al., Running neutrino nasses, mixings and CP Phases: Analytical results and phenomenological consequences, Nucl. Phys. B **674**, 401 (2003).

[47] P. H. Chankowski, Z. Płuciennik, Renormalization group equations for seesaw neutrino masses, Phys. Lett. B **316**, 312 (1993).

[48] K. S. Babu et al., Renormalization of the neutrino mass operator, Phys. Lett. B **319**, 191 (1993).